Imaging and X-ray Microanalysis of a Poly(ethylene-*ran*-methacrylic acid) Ionomer Melt Neutralized with Sodium

Andreas Taubert and Karen I. Winey*

Laboratory for Research on the Structure of Matter and Department of Materials Science and Engineering, University of Pennsylvania, Philadelphia, Pennsylvania 19104-6272

Received March 15, 2002; Revised Manuscript Received June 28, 2002

ABSTRACT: The ionic aggregates in an as-extruded and a recrystallized poly(ethylene-*ran*-methacrylic acid) ionomer melt neutralized with sodium have been imaged using scanning transmission electron microscopy (STEM). The recrystallized sample exhibits a macrophase-separated structure with three phases with distinct boundaries. Phase I does not contain aggregates > 1 nm, phase II contains small spherical aggregates of ∼2−15 nm in diameter, and phase III contains large aggregates with diameters ranging from ∼20 to 160 nm. Contrast reversal between bright field and annular dark field STEM images indicates that the aggregates are Na-rich. In contrast, the as-extruded sample is featureless on the STEM length scale. This study shows that thermal history has a major impact on ionomer morphology. X-ray energy dispersive spectroscopy (XEDS) using a 1 nm probe confirms higher Na contents in the ionic aggregates and detects Na in the matrix. XEDS also finds a significant amount of C in the ion-rich aggregates due to the incorporation of PE and unneutralized MAA monomers into the aggregates. The observed phase separation in the recrystallized sample complicates the interpretation of scattering and spectroscopic data, but we attempt to reconcile our findings with previous studies.

Introduction

Poly(ethylene-*ran*-methacrylic acid) (EMAA) ionomers neutralized with different metal cations have been marketed by DuPont for over three decades under the trade name Surlyn. They have found use in packaging, coatings, adhesives, and other fields. The presence of ionic aggregates in these semicrystalline ionomers has a major impact on their physical properties and has therefore been a subject of continuing research within the polymer community. Despite the large effort in understanding structure formation and structure−property relations in ionomers, there are still unresolved questions. As more advanced analytical techniques become available, research in the ionomer field has seen an increasing amount of data, but a unified description of ionomers remains to be developed.

A variety of spectroscopic techniques have been used to explore the local (<1 nm) environments of the neutralizing cations in ionomers: solid-state NMR (SSNMR),[1−6] FTIR,[7−14] dielectric,[15] and EXAFS.[10,11,16−24] The majority of the data suggests that neutralized acids and their cations exist both in aggregates and as isolated species. For example, dielectric spectroscopy[15] of Na-neutralized noncrystalline EMAA ionomers found two relaxation processes that are ascribed to long chain segments containing Na carboxylates isolated in the matrix and to segments containing Na carboxylates incorporated in ionic aggregates. Also, ^{23}Na SSNMR of Na-neutralized sulfonated poly(styrene) (Na-SPS) detects a narrow peak at 7 ppm and a broad peak ∼−20 ppm that reportedly correspond to isolated and aggregated Na^+, respectively. O'Connell et al.[3] suggest that the breadth of the signal at ∼−20 ppm in the ^{23}Na SSNMR spectra of Na-SPS is due to variations within the aggregated cations, which arise from dimers, trimers, etc. Kuwabara and Horii report that ^{23}Na SSNMR spectra of a Na-EMAA ionomer only exhibit one broad signal at −12 ppm, which is independent of the thermal history of the sample, though these authors did not speculate about peak width.[6] Farrell and Grady performed EXAFS studies on a Na-neutralized EMAA with 4 mol % methacrylic acid. Interestingly, the uniformity of the Na environment decreases with increasing degree of neutralization, suggesting multiple local environments.[18] A recent FTIR study of EMAA ionomers neutralized with various cations shows that the number of unneutralized acids associated with neutralized acids depends on both the cation type and the degree of neutralization.[14]

The morphology of the ionic aggregates has mainly been investigated by interpreting small-angle X-ray scattering (SAXS) patterns.[25−41] Typical features of SAXS data from an ionomer include a broad scattering peak at q values of ∼0.5−4 nm^{-1} and a low-angle upturn close to the beam stop. The origin of the scattering peak is assigned to the size, shape, and spatial distribution of the ionic aggregates, although there are conflicting models that claim to accomplish this. Yarusso and Cooper ascribe the low-angle upturn to artifacts such as parasitic scattering, precipitated neutralizing agent, or other impurities.[30,31] Williams et al.[42] associate the upturn with the inhomogeneous distribution of multiplets as introduced by Eisenberg et al.[32] More recent anomalous SAXS experiments[28,29,38−40] suggest that both the scattering peak and the low-angle upturn are associated with the presence of the neutralizing cations in the ionomers and not to impurities. Ding et al.[38] suggest a nonrandom distribution of unaggregated ionic groups in the matrix as the source of the low-angle upturn. Wu et al.[39] suggest that long-range inhomogeneities cause the upturn; the inhomogeneities might be "some Zn salts or ion-cluster domains or inhomogeneities in the ionic background". They also suggest the sample preparation by compression molding or nonequilibrium structures due to the short annealing time as possible sources of the upturn. Register and Cooper assign the upturn to the microphase-separated structure of ion-rich aggregates, amorphous matrix, and crystal-

10.1021/ma0203952 CCC: $22.00
Published on Web 08/08/2002

line matrix, where applicable.[28,29] Li et al.[43] used ultra small-angle X-ray scattering (USAXS) to investigate Zn-SPS and concluded that there are long-range metal concentration variations causing the upturn; the most likely source of these concentration variations is thought to be compositional variations in the SPS. Though powerful in some regards, scattering and spectroscopy methods are difficult to apply in the absence of complementary imaging techniques that validate their morphological models, particularly in complex heterogeneous materials.

Imaging methods can yield valuable information about ionomer morphology, because imaging provides a model-independent determination of the presence, size, size distribution, shape, shape variation, and spatial distribution of the ionic aggregates. For example, recent atomic force microscopy (AFM) investigations found spherical aggregates in the amorphous regions of Zn- and Na-neutralized EMAA ionomers.[44,45] Early transmission electron microscopy (TEM) experiments have, however, yielded ambiguous and even misleading information about ionomer morphology.[46] Using scanning transmission electron microscopy (STEM), where the contrast scales approximately with the atomic number squared, Z^2,[47−49] rather than TEM, our group has successfully imaged ionic aggregates in various amorphous and semicrystalline ionomers. Semicrystalline Zn-EMAA ionomers contain spherical aggregates of ∼2 nm in diameter randomly distributed in the polymer matrix.[50,51] Amorphous Zn-SPS[52,53] and Cs-neutralized poly(styrene-*ran*-methacrylic acid) (Cs-SMAA)[54] exhibit macrophase separation with regions containing spherical and/or vesicular aggregates and regions without detectable aggregates. While STEM experiments demonstrate that ionomers possess a diversity of ionic aggregates that was not anticipated from the spectroscopy and scattering data, ionomer morphologies are still far from understood.

In this paper, we report the morphology and local chemical composition of a Na-neutralized EMAA ionomer using both STEM imaging and X-ray energy-dispersive spectroscopy (XEDS). This is noteworthy because only recently has the detection of small amounts of light elements become possible in STEM, e.g., P (Z = 15) in biological samples[55] or P segregating to interfaces in steels.[56] Similar to biological samples, our experiments on a Na-neutralized ionomer have the difficulty that both the matrix and ionic aggregates possess low atomic number species: C (Z = 6), O (Z = 8), and Na (Z = 11). This yields a small atomic number *difference* between the Na-rich aggregates and the matrix that mostly consists of C, thereby limiting contrast in these STEM experiments. To our knowledge, this is the first STEM study of a Na-neutralized ionomer. The imaging experiments were augmented by XEDS using a 1 nm probe to qualitatively determine the local Na content of both the aggregates and matrix. The combination of STEM with analytical techniques such as XEDS provides a powerful approach for investigating complex materials with chemical heterogeneity on a length scale from a nanometer to hundreds of microns.

Finally, a comment about terminology. In our experimental studies, we use the term "aggregate" to describe an ion-rich entity in an ion-poor polymer matrix. Aggregates do not directly correspond to either "multiplets" or "clusters" as defined by Eisenberg et al.,[32] because these terms from the Eisenberg−Hird−Moore model impose restrictions on their composition and/or size. We use the term "matrix" to describe regions in which aggregates are not detected using STEM imaging.

Experimental Section

Materials and Sample Preparation. As-extruded pellets of partially Na-neutralized poly(ethylene-*ran*-methacrylic acid) (EMAA) ionomers were provided by Dr. John Paul of DuPont. The EMAA copolymer was synthesized via high-pressure free radical copolymerization yielding a polymer with 5.4 mol % methacrylic acid, 83% of which were neutralized with Na^+ in a melt neutralization process by DuPont. This ionomer is a research grade material and has previously been investigated by Grady et al.[18] and Register et al.[57−59] Here, it was investigated both in the as-extruded state as received from DuPont and after isothermal crystallization from the melt. Recrystallization was accomplished in a hot press at 5000 psi by (1) melting the sample at 130 °C for 90 min, (2) rapidly cooling (∼5 min), and (3) isothermally crystallizing for 270 min at 60 °C. The sample was then removed from the hot press, quenched with liquid nitrogen, and stored at 4 °C. Thin sections for STEM with nominal section thicknesses of 25 or 40 nm were obtained at −80 °C with a dry diamond knife and transferred to gold specimen grids. The grids were stored in a vacuum at 25 °C prior to the STEM experiments.

Scanning Transmission Electron Microscopy. STEM experiments were performed on a JEOL 2010F field emission electron microscope operated at 200 kV and equipped with a Gatan bright field (BF) and a JEOL annular dark field (ADF) detector. We used a 50 μm condenser aperture, an ADF collection angle of ∼40 mrad, and a probe size of 0.2 nm.[60] The sample was maintained at a vacuum of $\sim 2 \times 10^{-5}$ Pa during STEM experiments. Magnifications ranged from 50 000 to 1 200 000×. The image acquisition time was 21 s. Except for some carbon contamination, the samples looked identical before and after image acquisition; we therefore conclude that the electron beam does not measurably alter the morphology of the material. Image analysis was performed with Adobe Photoshop 5 using standard procedures, including background correction, gray level adjustments, and contrast enhancement. For aggregate size determination, over 300 aggregates were measured from more than 10 images using the "measure" tool in Photoshop.

X-ray Energy Dispersive Spectroscopy. X-ray energy dispersive spectroscopy (XEDS) experiments were performed in the JEOL 2010F equipped with a Princeton Gamma Tech (PGT) X-ray energy dispersive spectrometer. Spectra were acquired by placing a stationary 1 nm probe at the point of interest and collecting a spectrum for 100 s. Longer acquisition times contaminate the sample and do not significantly improve the quality of the spectra. In addition, smaller probe size give insufficient signal-to-noise ratios. Data analysis was performed with the IMIX software (PGT); after background subtraction, the individual C *K* (282 eV) and Na *K* (1072 eV) lines from the sample and the Au *M* (M_4, 2291 eV; M_5, 2205 eV; not observed as single lines) lines from the grid were deconvoluted using IMIX routines and the integrated counts were recorded. The O *K* line (523 eV) was obscured by the intense C *K* line and could not be analyzed. Occasionally, Si *K* (1839 eV) lines from the detector were also observed.

Small-Angle X-ray Scattering. Small-angle X-ray scattering (SAXS) experiments in a q range from ∼0.25 to 3.7 nm^{-1} were performed on both the as-extruded and recrystallized samples. We used our recently commissioned multiple angle X-ray scattering (MAXS) apparatus, which we describe here. A Nonius FR591 rotating anode X-ray generator operates at 40 kV and 85 mA with a copper anode and a 2 × 0.2 mm spot size. Doubly focusing mirror−monochromator optics (Molecular Metrology, Inc.) provide 1:1 focusing of the Cu $K\alpha_1$ radiation (λ = 1.5408 Å) at the detector, resulting in both high flux at the sample and high angular resolution. A Bruker HiStar multiwire detector provides highly sensitive area detection with low dark current. An integral vacuum exists between the generator and the detector, with a Be window at each end and

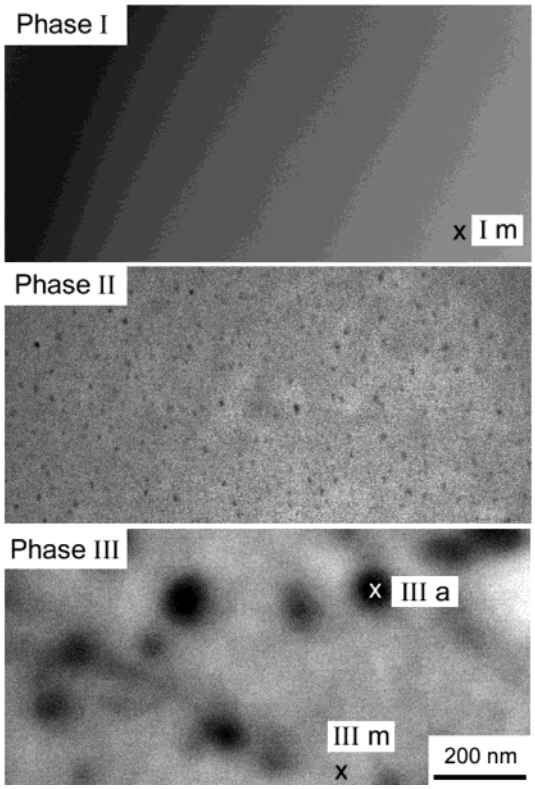

Figure 1. Bright field STEM images of Na-EMAA showing three distinct phases. Phase I is featureless on the STEM length scale, phase II contains small spherical aggregates, and phase III contains large spherical aggregates. The designations "a" and "m" denote the locations of spot XEDS spectra of the aggregate and the matrix, respectively, presented in Figures 5 and 7.

a Kapton window to support the beam stop. Silver behenate was used for angular calibration. The 2D data were integrated over 270°. A background collected and integrated under the same conditions was subtracted from the sample data.

Results

The partially Na-neutralized EMAA ionomer exhibits three distinct phases after recrystallization as shown by the bright field (BF) STEM images in Figure 1. Phase I does not exhibit aggregates on the STEM length scale. The dark region on the left of Figure 1 (top) is due to a thickness variation. Phases II and III both contain spherical aggregates as indicated by circular features with aspect ratios of ∼1 in the STEM images. The spherical aggregates are randomly arranged in the matrix, and the aggregates in phase II are smaller on average than the aggregates in phase III; more on aggregate sizes below.

Phase boundaries were detected between the three phases described above, further supporting the identification of multiple phases. Figure 2 is an example of a phase boundary between phase I (top left of image) and phase III (large spherical aggregates, bottom of image). Note that there are a few spherical aggregates in phase I near the boundary region, though further from the boundary no aggregates are found. This and similar images of phase boundaries ensure that phase I is indeed featureless on the STEM length scale and not simply out of focus. The three phases extend over at least several hundred nanometers and are present in all the microtomed sections investigated. We therefore conclude that the three-phase morphology described here is representative of the bulk morphology in recrystallized Na-EMAA. In the following, we will investigate the sizes of the spherical aggregates and the chemical composition of each region in the recrystallized sample.

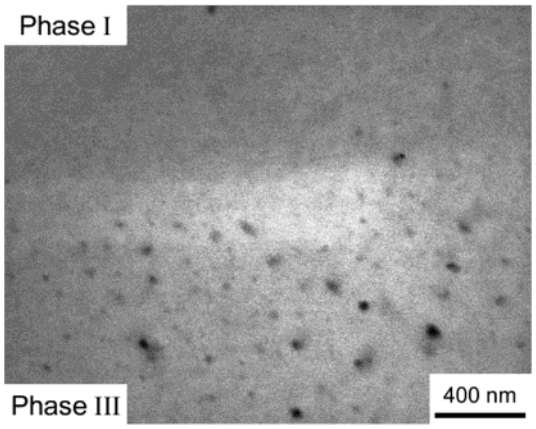

Figure 2. STEM BF image of a phase boundary between phases I (top left) and III (bottom). Some aggregates are found in phase I close to the phase boundary, but none are detected further from the phase boundary.

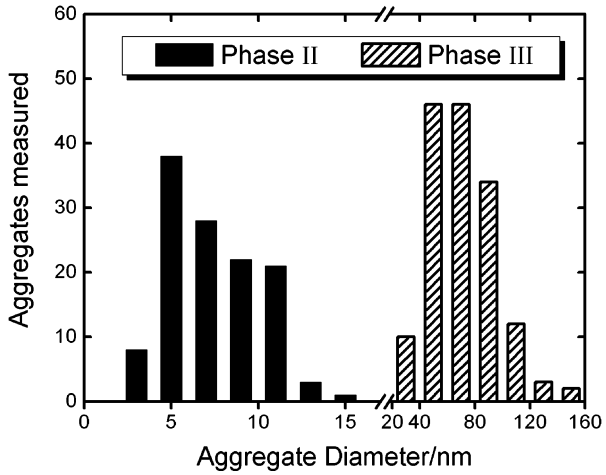

Figure 3. Histogram of the aggregate diameters for phases II and III. Note the change of scale on the *x*-axis. The smaller aggregates were found exclusively in regions designated as phase II, while the larger aggregates correspond to phase III.

Figure 3 shows a histogram for the aggregate diameters in the recrystallized Na-neutralized EMAA ionomer; note the change in scale along the *x*-axis. No aggregates with diameters less than ∼2 nm or between 14 and 20 nm were found. The aggregate diameter distribution in the recrystallized sample is clearly bimodal, and the two populations are spatially separated. The smaller aggregates are exclusively found in regions designated as phase II and have a mean diameter of ∼6.9 nm. Conversely, the larger aggregates are found only in regions designated as phase III and have a mean diameter of ∼69 nm. Because there is no region in the sample containing *both* small and large aggregates, we make the distinction between phases II and III.

At this point it is important to discuss the detection limits of STEM. The smallest aggregates we can confidently detect are ∼1 nm in this particular material, Na-EMAA. Thus, our designation of phase I as featureless refers to the absence of aggregates larger than ∼1 nm in diameter. This detection limit is for Na but improves with higher atomic number in accordance with the

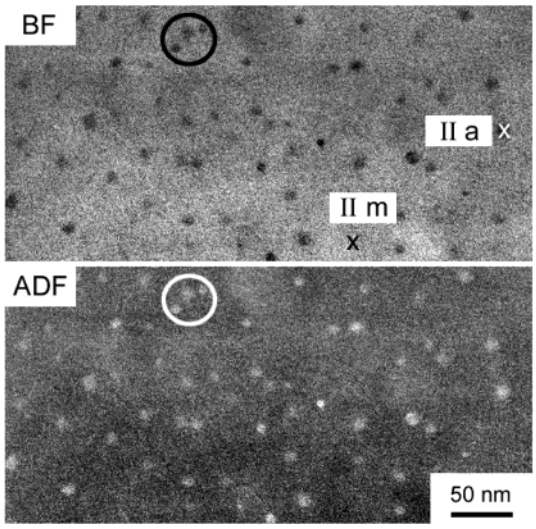

Figure 4. Bright field (BF) and annular dark field (ADF) image of the same area in phase II demonstrating contrast reversal due to higher Na concentration in the aggregates than in the matrix. The circles highlight three representative aggregates to facilitate the comparison of the two images. The designations "a" and "m" denote the locations of spot XEDS spectra of the aggregate and the matrix, respectively, presented in Figure 6.

contrast formation mechanism in STEM.[47−49] In addition, the STEM specimens are not infinitely thin; therefore, two or more aggregates located at different heights in the specimen may overlap in the image and suggest one larger entity because the image is a two-dimensional projection of a three-dimensional structure. However, given the uniformity of the aspect ratios of the features, overlap does not appear to be substantial.

Because the electron scattering in STEM is approximately proportional to Z^2,[47−49] regions with a higher average Z appear dark in the STEM BF images and bright in the ADF images. Figure 4 shows a pair of BF/ADF images of phase II with a one-to-one correspondence between the dark spots in the BF image and the bright spots in the ADF images. This contrast arises because the Na ($Z = 11$) atoms scatter more electrons to higher angles than the polymer matrix consisting predominantly of C ($Z = 6$). Similar BF/ADF pairs were obtained from the large aggregates in phase III, whereas for the featureless phase I neither BF nor ADF images showed any contrast, except that due to thickness variations, which are on a much larger length scale than ionic aggregates. The BF/ADF pairs indicate that the aggregates in phase II and III have a higher average Z than the matrix because they are Na-rich with respect to the matrix.

We used XEDS spot analysis to qualitatively assess the local chemical compositions of phase I and the aggregates (labeled "a") and the matrices (labeled "m") in phases II and III. The spectra were collected by placing a focused electron beam of ∼1 nm in diameter at the locations indicated in Figures 1 (top, bottom) and 4 (top). The featureless phase I contains a measurable amount of Na, even though no aggregates were detected in STEM (Figure 5). In both phases II and III, the aggregates exhibit a higher Na X-ray signal than the adjacent matrix (Figures 6 and 7). We compare the integrated Na X-ray counts obtained from spot spectra recorded on several aggregates and matrix points from a single field of view for each phase to minimize the effect of specimen thickness variations. Note that the

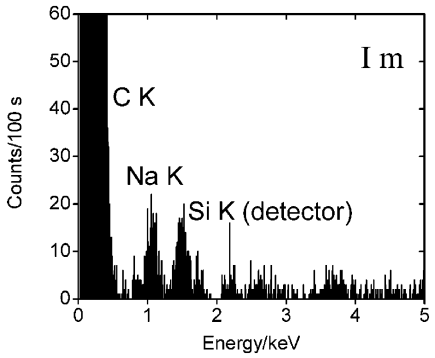

Figure 5. Spot XEDS spectrum taken from phase I as indicated in Figure 1 (I m). Na is present even though the STEM image is featureless.

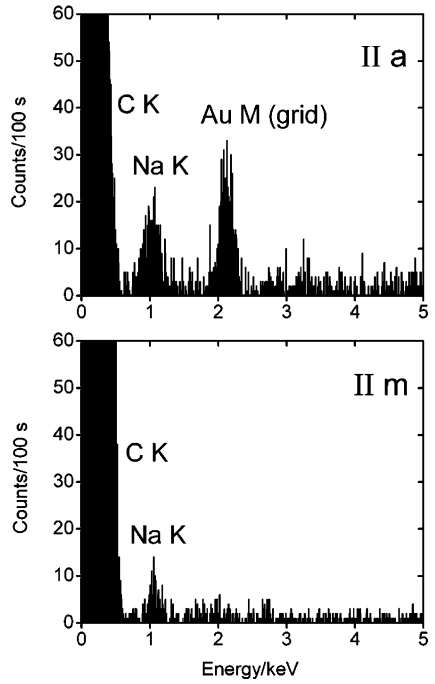

Figure 6. Spot XEDS spectra taken from an aggregate (II a) and from the matrix (II m) in the small aggregate-phase II (see Figure 4). More Na is present in the aggregate.

"aggregate" spectra also have contributions from the matrix, because the electron beam passes through both matrix and aggregate, as explained in more detail in the next paragraph. The ratios of integrated Na counts ($\text{Na counts}_{\text{aggregate+matrix}}/\text{Na counts}_{\text{matrix}}$) are ∼1.3 for the small aggregate-phase II and ∼1.7 for the large aggregate-phase III, indicating that the aggregates contain more Na than the matrix. These composition variations are consistent with our interpretation of the STEM images given above, namely that phases II and III contain Na-rich aggregates in recrystallized Na-EMAA.

A spot XEDS spectrum collected by placing the probe on an aggregate records the *sum* of the Na *K* counts arising from Na in both the aggregate and the matrix that the electrons encounter while passing through the microtomed section of ionomer. Thus, the difference in the ratios of integrated counts between phase II and phase III cannot be interpreted as difference in aggregate composition, because the aggregates are of different average size. For example, phase II contains aggregates that are much smaller (mean diameter 6.9 nm) than the section thickness (25−40 nm), as schematically shown in Figure 8a. Therefore, the XEDS

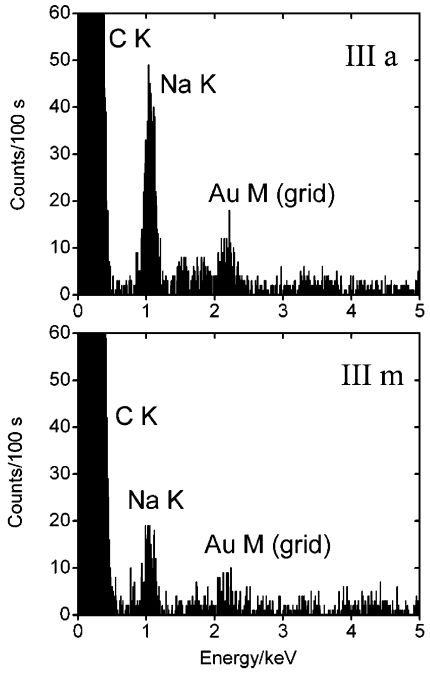

Figure 7. Spot XEDS spectra taken from an aggregate (III a) and from the matrix (III m) in the large aggregate-phase III (see Figure 1). As in phase II, Na is present in the matrix, but the Na concentration is higher in the aggregate.

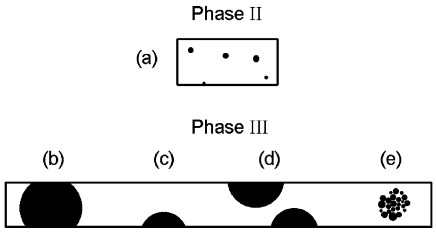

Figure 8. Schematic of a cross section of a STEM sample depicting (a) small aggregates in phase II and aggregates in phase III, (b) a large aggregate spanning the entire section thickness, (c) a large aggregate spanning a fraction of the section thickness, (d) two overlapping large aggregates, and (e) a collection of many small aggregates. Cases b−e are indistinguishable in the STEM.

spectra reflect primarily the composition of the matrix. In contrast, the large aggregates (mean diameter 69 nm) of phase III present several possibilities. One might probe an aggregate that spans the entire section thickness (Figure 8b), so that the XEDS spectrum is indicative of the aggregate composition alone. Alternatively, a large aggregate in phase III might span only a portion of the section (Figure 8c), which requires that we independently determine the relative path lengths (matrix:aggregate) before interpreting the XEDS spectra further. Yet other alternatives are that two or more aggregates overlap in the two-dimensional image and appear to be a larger aggregate (Figure 8d) or that the large aggregates consist of many small aggregates that cannot be resolved in the STEM (Figure 8e). Unfortunately, the situations illustrated in Figure 8b−e are indistinguishable in a STEM image, so the composition of the Na-rich aggregates in phase III cannot be determined. However, it is satisfying that the relative amount of Na (matrix:aggregate) is larger in the case of phase III where the Na-rich aggregates are 10 times larger on average than in phase II and therefore are likely to contribute to a greater extent to the XEDS spectra.

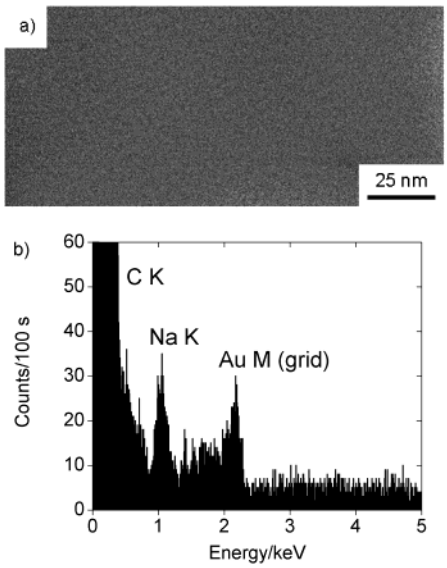

Figure 9. BF STEM image of an as-extruded Na-EMAA ionomer (a). No aggregates are visible on the STEM length scale, but the corresponding XEDS (b) exhibits an Na *K* line.

We will now discuss the implications of the aggregate sizes. An idealized Na carboxylate is ∼0.3 nm across; thus, aggregates consisting only of Na carboxylates should not exceed a diameter of ∼0.6 nm. The observed radii of the Na-rich aggregates are considerably larger than this even in phase II. In addition, the C *K* line intensity recorded on an aggregate that spans the whole section thickness (Figure 8b) should drop dramatically relative to the C *K* line intensity of the adjacent matrix if the aggregates contained exclusively ionic species. However, even in phase III where the aggregates on average span more than half of the thin section, there is no significant drop in the C *K* line intensity. Thus, the size and the nearly constant C *K* line intensities in XEDS indicate that the aggregates contain more than Na^+COO^-; that is, they apparently incorporate ethylene and/or unneutralized methacrylic acid monomeric units. A recent IR study found unneutralized acid groups associated with neutralized Na carboxylates.[14] The incorporation of the unneutralized acid groups into the aggregates results in aggregates that are larger and contain more C than the Na carboxylate alone, consistent with our STEM and XEDS data. Nonionic monomeric units in the aggregates reduce the STEM contrast (which is based on average atomic number) between the matrix and the aggregates relative to that expected from entirely ionic aggregates.

When the aggregates of phase II and phase III are viewed at the same magnification, as in Figure 1, the aggregate boundaries appear broader for the large aggregates. This could be the result of physically more diffuse boundaries. However, broader boundaries also result from projecting larger spheres to a two-dimensional image. Because the STEM images are two-dimensional projections of a three-dimensional structure, we cannot distinguish between these possibilities.

In contrast to the three-phase morphology of the recrystallized sample, the as-extruded Na-EMAA sample exhibits only one phase on the STEM length scale (Figure 9a). Both BF and ADF STEM images of the as-extruded Na-EMAA ionomer are featureless throughout the sample. The morphology is comparable to phase I in the recrystallized sample. Similar to phase I in the

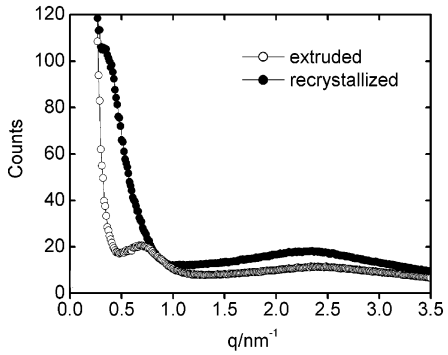

Figure 10. SAXS patterns of the as-extruded and the recrystallized Na-EMAA ionomer. The broad peak at higher *q* values is traditionally assigned to the ionic aggregates, and the low-angle peak is due to poly(ethylene) crystallinity.

recrystallized ionomer, the XEDS spectra of the as-extruded pellets detect Na in the absence of detectable aggregates (Figure 9b). A broad peak is evident in the SAXS pattern of both samples: $\sim$2.45 nm^{-1} (as-extruded) and 2.33 nm^{-1} (recrystallized) (Figure 10). This peak position is typically associated with the presence of ionic aggregates; however, STEM detects ionic aggregates in the recrystallized sample only. The lower angle peaks arise from polyethylene crystallinity: $\sim$0.7 nm^{-1} (as-extruded) and 0.45 nm^{-1} (recrystallized).

Discussion

The as-extruded, partially neutralized Na-EMAA ionomer is featureless when imaged using either BF or ADF STEM. The STEM resolution in this Na-neutralized material is $\sim$1 nm, so we cannot exclude the presence of smaller aggregates in this material. In contrast, STEM experiments on as-extruded Zn-neutralized EMAA ionomers show nearly monodisperse, spherical, Zn-rich aggregates randomly distributed within the polymer matrix.[50,51] Both Na- and Zn-neutralized ionomers were prepared by DuPont from the same batch of EMAA random copolymer via melt neutralization. Thus, the simple change of cation from Zn^{2+} to Na^{+} is apparently sufficient to impede the formation of ionic aggregates > 1 nm during melt neutralization. Further experiments are necessary to understand the influence of the neutralizing cation.

The recrystallized Na-EMAA ionomer investigated here exhibits a complex three-phase morphology. Phase I is homogeneous on the STEM length scale as described above for the as-extruded materials. Phase II and phase III both exhibit via STEM Na-rich spherical aggregates randomly distributed within the phase, but the phases contain different size populations. Namely, phase II possesses aggregates <15 nm in diameter, while phase III possesses aggregates 20−160 nm in diameter. Qualitative XEDS analysis suggests that the Na-rich aggregates contain C in excess of that in a Na carboxylate. The excess carbon could arise by having ethylene monomeric units and/or unneutralized acid groups incorporated into the aggregates.

According to XEDS, phase I and the matrices in phases II and III of the recrystallized sample contain a measurable amount of Na. This result indicates that there are isolated Na carboxylates and/or very small aggregates that are not detectable by STEM in these melt-neutralized materials. Thus, as suggested previously by various bulk spectroscopy methods,[2−6,14,15,18] nanometer-scale XEDS finds that the Na^{+} ions in the recrystallized sample can exist in a variety of local environments including isolated Na carboxylates and/or very small ion-rich aggregates (all phases), small spherical aggregates (phase II), and large spherical aggregates (phase III).

The presence of three phases but only two components (EMAA random copolymer and Na cations) indicates that the recrystallized material is not in equilibrium. An alternative explanation could be that the macrophase separation is due to variations in molecular weight and/or acid content of the poly(ethylene-*ran*-methacrylic acid) random copolymer. For example, random copolymers can phase separate when their compositions vary sufficiently. Note that the same EMAA copolymer was used to prepare the previously studied Zn-neutralized EMAA ionomers, which does not exhibit macrophase separation. Thus, it is more likely that the three-phase morphology is the result of processing, which we will discuss next.

The EMAA base polymer was neutralized by DuPont in the melt state at elevated temperature and pressure. Perhaps, the mixing of the EMAA and the neutralizing agent was insufficient to homogeneously distribute the latter in the EMAA during neutralization. Such processing conditions may lead to regions with low and others with higher neutralization levels. The temperature, pressure, and rate of extrusion and subsequent quenching of the melt neutralization process might also prevent (or at least severely limit) ionic aggregation and thus lead to the observed morphology of the as-extruded material. Researchers using IR and EXAFS spectroscopy[24] have recently found that the Zn coordination of a partially neutralized EMAA ionomer changes from hexacoordination to tetracoordination as the pressure increases from 0 to 5 MPa. This indicates that the melt processing at elevated temperature and pressure may affect the microstructure of ionomers. Isothermal, quiescent recrystallization may then allow for chain rearrangement and ionic aggregation within regions of different neutralization levels.

Regardless of the origin of the three-phase morphology in the recrystallized Na-EMMA, the complexity of the morphology significantly complicates the interpretation of bulk measurements, such as spectroscopy, scattering, and dynamic mechanical analysis. For example, the low-angle upturn in the SAXS patterns in Figure 10 probably has contributions from both the macrophase separation and the large aggregates in phase III that will be difficult, if not impossible, to separate. The contribution of the aggregates in phase II may be hidden in the signal of the poly(ethylene) lamellae at lower scattering angles. STEM has the advantage that the shape, size, and spatial distribution of ion-rich aggregates above a certain size can be determined model-free. STEM also has limitations with respect to the detection of very small or overlapping aggregates because the STEM images are two-dimensional projections of the polymer microstructure. Our experiments therefore demonstrate that spectroscopy and scattering experiments are complementary with direct imaging experiments and should be used in combination.

We now compare our findings with other results on Na-EMAA ionomers. Recall that our Na-EMAA has 5.4 mol % acid and is neutralized to 83%. In all these comparisons, the details of the thermal history and processing vary. Clearly, the results in this paper

illustrate the profound influence of processing on ionomer morphology. Consequently, these comparisons are qualitative.

Sauer and McLean investigated the morphology of Na-EMAA ionomers using AFM.[44] Their EMAA copolymers, containing 4.9 and 7.4 mol % acid monomer and neutralized to 54 and 59%, were melt pressed at 180 °C and cooled to room temperature. Using tapping mode AFM, they detect spherical aggregates of ~2 nm in diameter, but no large aggregates or multiphase structure. There are several possible reasons for the differences between our STEM data and the AFM results. (1) The hardness of the large aggregates we observe in STEM may be similar to the hardness of the matrix because they incorporate a large amount of polymer backbone. Therefore, AFM was unable to detect the large aggregates. (2) AFM probes the near surface region, while STEM probes the bulk. Because of surface effects, perhaps phase separation and large aggregates do not exist close to the surface. (3) The field of view in the AFM is smaller, and therefore only one phase was detected.

Tsujita et al.[41] have used the original Yarusso–Cooper model[30,31] to analyze the SAXS patterns of various Na-EMAA ionomers that were neutralized via soaking in methanolic NaOH. In particular, two Na-EMAA ionomers that are similar to our material (3.5 mol % MAA, 80% neutralized and 5.4 mol % MAA, 82% neutralized) were found to have aggregate diameters of ~1.4 nm. The scattering peaks for these samples are located at ~2.2 nm^{-1}, which is similar to our scattering peak positions (Figure 10). The aggregate sizes obtained by Tsujita et al. are also similar to the values obtained by Sauer and McLean, but because the SAXS patterns were interpreted with the Yarusso–Cooper model, which does not account for multiple phases, no information about the presence of multiple phases is available from the Tsujita study.

Farrell and Grady find a decrease in the uniformity of the Na environment with increasing degree of neutralization in the EXAFS spectra of a series of Na-neutralized EMAA with 4 mol % acid monomer.[18] Kuwabara and Horii report a broad signal centered at −12 ppm in the ^{23}Na SSNMR spectra of a 60% neutralized Na-EMAA with 5.4 mol % acid monomer,[6] similar to a broad signal observed in the ^{23}Na SSNMR spectra of 23% and 54% neutralized Na-EMAA.[1] Kuwabara and Horii demonstrate that the position and the breadth of this signal are invariant to annealing near the melting point of the poly(ethylene), indicating no significant structural changes on the length scale of the individual Na cations with thermal treatment.[6] A similarly broad signal in the ^{23}Na SSNMR spectra of Na-SPS has been assigned to a distribution of local cation environments,[3] but Kuwabara and Horii did not elaborate on the implications of the breadth of the signal. Although these spectroscopic techniques probe a shorter length scale than STEM that is insensitive to aggregate size and multiphase structures, they qualitatively concur with our findings of a complex morphology with different Na environments.

It should be stressed again at this point that all samples compared here have a different thermal history, and the data obtained with these different techniques strongly suggest that thermal history is one of the key parameters that governs ionomer morphology. Clearly, inconsistencies remain between the interpretations of spectroscopic, scattering, and imaging data; these will have to be resolved in order to develop a unified description of ionomer morphology.

Conclusion

This article demonstrates that STEM and XEDS are powerful methods for investigating ionomers containing light elements, such as sodium. The featureless morphology of the as-extruded Na-EMAA ionomer investigated here differs profoundly from the spherical Zn-rich aggregate morphology found previously in as-extruded Zn-EMAA ionomers melt neutralized from the same EMAA copolymer. The recrystallized Na-EMAA contains three distinct phases. Phase I is featureless on the STEM length scale, phase II contains small spherical aggregates, and phase III contains large spherical aggregates. Both the aggregates and the matrices contain a measurable amount of Na. STEM and XEDS therefore show that the Na^+ ions exist in a variety of local environments as is consistent with previous ^{23}Na SSNMR and EXAFS studies. Furthermore, this study presents evidence for the incorporation of PE and unneutralized MAA monomeric units into the aggregates. Finally, this paper presents discrepancies in the morphologies of Na-EMAA ionomers that exist in the literature, the origin of which probably arises from both experimental methods and sample preparation.

Acknowledgment. We acknowledge Prof. David B. Williams (Lehigh University) for technical discussions and Dr. John Paul (DuPont) for supplying the ionomer. We also thank Dr. Douglas M. Yates (Materials Characterization Facility, University of Pennsylvania) for technical assistance with the JEOL 2010F. Funding was provided by the Petroleum Research Foundation as administered by the American Chemical Society (ACS-PRF 34038-AC7), the National Science Foundation (NSF-DMR 99-06829), and DuPont.

References and Notes

(1) Dickinson, L. C.; MacKnight, W. J.; Connelly, J. M.; Chien, J. C. W. *Polym. Bull. (Berlin)* **1987**, *17*, 459.
(2) O'Connell, E. M.; Peiffer, D. G.; Root, T. W.; Cooper, S. L. *Macromolecules* **1996**, *29*, 2124.
(3) O'Connell, E. M.; Root, T. W.; Cooper, S. L. *Macromolecules* **1994**, *27*, 5803.
(4) O'Connell, E. M.; Root, T. W.; Cooper, S. L. *Macromolecules* **1995**, *28*, 3995.
(5) O'Connell, E. M.; Root, T. W.; Cooper, S. L. *Macromolecules* **1995**, *28*, 4000.
(6) Kuwabara, K.; Horii, F. *J. Polym. Sci., Part B: Polym. Phys.* **2002**, *40*, 1142.
(7) Coleman, M. M.; Lee, J.-Y.; Painter, P. C. *Macromolecules* **1990**, *23*, 2339.
(8) Brozoski, B. A.; Painter, P. C.; Coleman, M. M. *Macromolecules* **1984**, *17*, 1591.
(9) Ishioka, T. *Polym. J.* **1993**, *25*, 1147.
(10) Ishioka, T.; Shimizu, M.; Watanabe, I.; Kawauchi, S.; Harada, M. *Macromolecules* **2000**, *33*, 2722.
(11) Kutsumizu, S.; Nakumura, Y.; Yano, S. *Macromolecules* **2001**, *34*, 3033.
(12) Yano, S.; Nakamura, M.; Kutsumizu, S. *Chem. Commun.* **1999**, 1465.
(13) Kutsumizu, S.; Hara, H.; Tachino, H.; Shimabayashi, K.; Yano, S. *Macromolecules* **1999**, *32*, 6340.
(14) Walters, R. M.; Sohn, K. E.; Winey, K. I.; Composto, R. J. *J. Polym. Sci., Part B: Polym. Phys.*, submitted.
(15) Kutsumizu, S.; Tadano, K.; Matsuda, Y.; Goto, M.; Tachino, H.; Hara, H.; Hirasawa, E.; Tagawa, H.; Muroga, Y.; Yano, S. *Macromolecules* **2000**, *33*, 9044.
(16) Ding, Y. S.; Yarusso, D. J.; Pan, H. K.; Cooper, S. L. *J. Appl. Phys.* **1984**, *56*, 2396.
(17) Farrell, K. V.; Grady, B. P. *Macromolecules* **2000**, *33*, 7122.

(18) Farrell, K. V.; Grady, B. P. *Macromolecules* **2001**, *34*, 7108.
(19) Grady, B. P.; Cooper, S. L. *Macromolecules* **1994**, *27*, 6627.
(20) Grady, B. P.; Cooper, S. L. *Macromolecules* **1994**, *27*, 6635.
(21) Grady, B. P. *Macromolecules* **1999**, *32*, 2983.
(22) Grady, B. P.; Floyd, J. A.; Genetti, W. B.; Vanhoorne, P.; Register, R. A. *Polymer* **1999**, *40*, 283.
(23) Grady, B. P. *Polymer* **2000**, *41*, 2325.
(24) Hashimoto, H.; Kutsumizu, S.; Tsunashima, K.; Yano, S. *Macromolecules* **2001**, *34*, 1515.
(25) Jackson, D. A.; Koberstein, J. T.; Weiss, R. A. *J. Polym. Sci., Part B: Polym. Phys.* **1999**, *37*, 3141.
(26) Kutsumizu, S.; Tagawa, H.; Muroga, Y.; Yano, S. *Macromolecules* **2000**, *33*, 3818.
(27) MacKnight, W. J.; Taggart, W. P.; Stein, R. S. *J. Polym. Sci., Symp. Ser.* **1974**, *45*, 113.
(28) Register, R. A.; Cooper, S. L. *Macromolecules* **1990**, *23*, 310.
(29) Register, R. A.; Cooper, S. L. *Macromolecules* **1990**, *23*, 318.
(30) Yarusso, D.; Cooper, S. L. *Macromolecules* **1983**, *16*, 1871.
(31) Yarusso, D.; Cooper, S. L. *Polymer* **1985**, *26*, 371.
(32) Eisenberg, A.; Hird, B.; Moore, R. B. *Macromolecules* **1990**, *23*, 4098.
(33) Eisenberg, A.; Kim, J.-S. *Introduction to Ionomers*; John Wiley & Sons: New York, 1998.
(34) Marx, C. L.; Caulfield, D. L.; Cooper, S. L. *Macromolecules* **1973**, *6*, 344.
(35) Roche, E. J.; Stein, R. S.; Russell, T. P.; MacKnight, W. J. *J. Polym. Sci., Polym. Phys.* **1980**, *18*, 1497.
(36) Fujimura, M.; Hashimoto, T.; Kawai, H. *Macromolecules* **1981**, *14*, 1309.
(37) Chu, B.; Wu, D. Q.; MacKnight, W. J.; Wu, C.; Phillips, J. C.; LeGrand, A.; Lantman, C. W.; Lundberg, R. D. *Macromolecules* **1988**, *21*, 523−525.
(38) Ding, Y. S.; Hubbard, S. R.; Hodgson, K. O.; Register, R. A.; Cooper, S. L. *Macromolecules* **1988**, *21*, 1698.
(39) Wu, D. Q.; Chu, B.; Lundberg, R. D.; MacKnight, W. J. *Macromolecules* **1993**, *26*, 1000.
(40) Chu, B.; Wu, D. Q.; Lundberg, R. D.; MacKnight, W. J. *Macromolecules* **1993**, *26*, 994.
(41) Tsujita, Y.; Yasuda, M.; Makei, M.; Kinoshita, T.; Takizawa, A.; Yoshimizu, H. *Macromolecules* **2001**, *34*, 2220.
(42) Williams, C. E.; Russell, T. P.; Jerome, R.; Horrion, J. *Macromolecules* **1986**, *19*, 2887.
(43) Li, Y.; Peiffer, D. G.; Chu, B. *Macromolecules* **1993**, *26*, 4006.
(44) Sauer, B. B.; McLean, R. S. *Macromolecules* **2000**, *33*, 7939.
(45) McLean, R. S.; Doyle, M.; Sauer, B. B. *Macromolecules* **2000**, *33*, 6541.
(46) Handlin, D. L.; MacKnight, W. J.; Thomas, E. L. *Macromolecules* **1981**, *14*, 795.
(47) Pennycook, S. J. *Ultramicroscopy* **1989**, *30*, 58.
(48) Williams, D. B.; Carter, C. E. *Transmission Electron Microscopy-A Textbook for Materials Science*; Plenum Press: New York, 1996.
(49) Williams, C. E.; Colliex, C.; Horrion, J.; Jerome, R. *ACS Symp. Ser.* **1989**, *395*, 439.
(50) Laurer, J. H.; Winey, K. I. *Macromolecules* **1998**, *31*, 9106.
(51) Winey, K. I.; Laurer, J. H.; Kirkmeyer, B. P. *Macromolecules* **2000**, *33*, 507.
(52) Kirkmeyer, B. P.; Weiss, R. A.; Winey, K. I. *J. Polym. Sci., Part B: Polym. Phys.* **2001**, *39*, 477.
(53) Kirkmeyer, B. P.; Winey, K. I.; Weiss, R. A. *Microsc. Microanal.* **2000**, *6*, 1112.
(54) Kirkmeyer, B. P.; Taubert, A.; Kim, J.-S.; Winey, K. I. *Macromolecules* **2002**, *35*, 2648.
(55) Leapman, R. D.; Rizzo, N. W. *Ultramicroscopy* **1999**, *78*, 251.
(56) Papworth, A. J.; Watanabe, M.; Williams, D. B. *Ultramicroscopy* **2001**, *88*, 265.
(57) Vanhoorne, P.; Register, R. A. *Macromolecules* **1996**, *29*, 598.
(58) Quiram, D. J.; Register, R. A.; Ryan, A. J. *Macromolecules* **1998**, *31*, 1432.
(59) Tierney, N. K.; Register, R. A. *Macromolecules* **2002**, *35*, 2358.
(60) The probe sizes given in the paper are taken from the microscope settings as established by Dr. M. Kawasaki from JEOL, Inc.

MA0203952